"Cube-on-hexagon" orientation relationship for Fe on GaN(000$\bar{1}$): The missing link in bcc/hcp epitaxy

Cunxu Gao,[1,*] Oliver Brandt,[1] Steven C. Erwin,[2] Jonas Lähnemann,[1] Uwe Jahn,[1] Bernd Jenichen,[1] and Hans-Peter Schönherr[1]

[1]*Paul-Drude-Institut für Festkörperelektronik, Hausvogteiplatz 5-7, 10117 Berlin, Germany*

[2]*Center for Computational Materials Science, Naval Research Laboratory, Washington, DC 20375, USA*

(Received 7 May 2010; revised manuscript received 29 May 2010; published 9 September 2010)

We investigate, experimentally and theoretically, the epitaxy of body-centered-cubic Fe on hexagonal GaN. For growth on the Ga-polar GaN(0001) surface we find the well-known Pitsch-Schrader orientation relationship between Fe and GaN. On the N-polar GaN(000$\bar{1}$) surface we observe coexistence between the familiar Burgers orientation and a new orientation in which the Fe(001) plane is parallel to GaN(000$\bar{1}$). This "cube-on-hexagon" orientation constitutes the high-symmetry link required for constructing a symmetry diagram for bcc/hcp systems in which all orientation relationships are connected by simple rotations.

DOI: 10.1103/PhysRevB.82.125415 PACS number(s): 68.35.−p, 68.55.jm, 81.15.Hi, 61.05.jh

The crystallographic orientation relationship (OR) at the interface between two materials with different crystal structures plays a central role in materials science and technology. For example, the ORs found between bcc/fcc and bcc/hcp crystals resulting, e.g., from the martensitic transformations in the production of steel have been the subject of continuous research for almost one century because of their technological importance.[1–12] These ORs also govern the heteroepitaxy of many other metals, as well as various intermetallic and even nonmetallic materials.[13–19]

In view of their importance, Dahmen compiled an overview of all known bcc/fcc and bcc/hcp ORs.[20] Moreover, he constructed a unifying symmetry diagram for bcc/fcc epitaxy that connects the observed ORs by simple rotations. But for bcc/hcp epitaxy he was unable to construct such a diagram because of the "lack of a high-symmetry OR such as the Bain OR for the fcc case."[20]

Bauer and van der Merwe subsequently showed that most ORs could be understood in terms of simple, purely geometrical considerations based on the most densely packed rows of the two lattices.[21] However, even these considerations did not lead to the missing high-symmetry bcc/hcp orientation connecting the widely observed Pitsch-Schrader (PS) (Ref. 8) and Burgers (B) ORs.[4]

In this paper we report the experimental observation of this high-symmetry OR for Fe on GaN(000$\bar{1}$). Specifically, we observe domains with α-Fe(001)$\langle 010\rangle \| $GaN(0001)$\langle 11\bar{2}0\rangle$. On GaN(000$\bar{1}$) this "cube-on-hexagon" (CoH) orientation coexists with the Burgers OR. In contrast, on GaN(0001) a pure Pitsch-Schrader OR is observed. Density-functional theory (DFT) calculations comparing the relative stability of these different ORs are consistent with these experimental results.

The epitaxial growth of both GaN and Fe was performed in a custom-built molecular-beam epitaxy (MBE) system equipped with solid-source effusion cells for Ga and Fe. Active nitrogen was provided by a radio-frequency N_2 plasma source. Nucleation and growth were monitored *in situ* by reflection high-energy electron diffraction (RHEED). A 300 nm GaN layer was grown by MBE on GaN(0001) templates and on Al_2O_3(0001) substrates to obtain Ga- and N-polar GaN surfaces (as ensured by RHEED),[22] respectively. Directly after growth of the GaN layer, excess Ga was desorbed prior to cooling down to the temperature at which Fe deposition was initiated (350 or 500 °C). Fe growth then occurred at the selected temperature with a rate of 0.12 nm/min to a final thickness of 30 nm. The OR between Fe and GaN was monitored *in situ* by RHEED "radar" scans[23] as described in detail previously.[24] The angular resolution of these scans is better than 0.4°. Electron backscatter diffraction (EBSD) was employed *ex situ* to obtain the crystal structure and orientational distribution of the Fe film in a direct and unambiguous way. EBSD maps visualize the domain structure of the Fe film on a nanometer spatial scale with an angular resolution better than 1°. Finally, the OR between Fe and GaN was assessed by high-resolution x-ray diffractometry (HRXRD). HRXRD longitudinal θ-2θ scans were recorded with a Ge analyzer crystal with a dynamic range of at least five orders of magnitude while azimuthal ϕ scans were taken with an open detector. The in-plane orientation distribution was measured with an angular resolution of 0.01°.

Figures 1(a) and 1(b) show RHEED radar scans of the surfaces of the Fe films grown at 350 °C on GaN(0001) and GaN(000$\bar{1}$) substrates, respectively. Figure 1(a) exhibits a

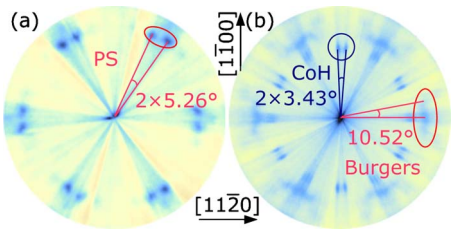

FIG. 1. (Color online) RHEED radar scans of the surfaces of the Fe films grown at 350° on (a) GaN(0001) and (b) GaN(000$\bar{1}$) substrates. The arrows refer to the in-plane directions of GaN(0001). The reflections belonging to a certain OR are circled for clarity. The angles given are those expected theoretically for the ideal ORs, not those measured in the pattern.

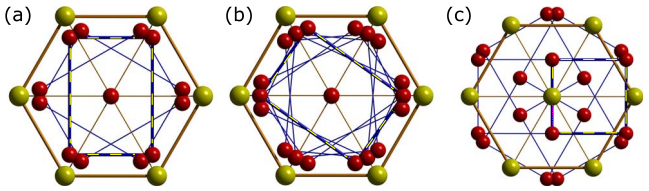

FIG. 2. (Color online) Schematic ball-and-stick models for Fe (dark) in the (a) Pitsch-Schrader, (b) Burgers, and (c) CoH ORs on the top Ga layer (light) of GaN{0001}. The models show a superposition of all symmetry-equivalent orientations (which in reality do not coexist in one unit cell) and the dashed rectangle highlights one of these orientations.

sixfold symmetry with two azimuthal maxima situated about $\pm 5°$ relative to GaN$\langle 11\bar{2}0\rangle$ in the ϕ direction as deduced from a comparison with the ϕ scan from the underlying GaN layer (not shown here). These maxima thus occur along the Fe$\langle 1\bar{1}\bar{1}\rangle$ and Fe$\langle 11\bar{1}\rangle$ directions, revealing Fe(101)$\langle 010\rangle \| $GaN(0001)$\langle 11\bar{2}0\rangle$, consistent with the Pitsch-Schrader OR. In contrast, Fig. 1(b) shows two distinct diffraction patterns with sixfold symmetry. For the first pattern three azimuthal maxima are found, at 0 and about $\pm 10°$ relative to GaN$\langle 11\bar{2}0\rangle$ in the ϕ direction, meaning that the maxima occur once again along the Fe$\langle 1\bar{1}\bar{1}\rangle$ and Fe$\langle 11\bar{1}\rangle$ directions. This in-plane orientation is the one expected for the Burgers OR between Fe and GaN, namely, Fe(101)$\langle 1\bar{1}\bar{1}\rangle \| $GaN(0001)$\langle 11\bar{2}0\rangle$ and Fe(101)$\langle 11\bar{1}\rangle \| $GaN(0001)$\langle 11\bar{2}0\rangle$. The second pattern exhibits two maxima about $\pm 3°$ relative to GaN$\langle 1\bar{1}00\rangle$ in the ϕ direction, and thus occurs along Fe$\langle 120\rangle$ and Fe$\langle \bar{1}20\rangle$. An orientation such that α-Fe(001)$\langle 010\rangle \| $GaN(0001)$\langle 11\bar{2}0\rangle$ would be consistent with the radial and angular location of these reflections. Because no OR matching these observations has been reported, we refer to it as cube-on-hexagon.

Figure 2 shows simple ball-and-stick models of the three ORs discussed here. For clarity, each of these views depicts only the local symmetry of the OR (which is reflected directly in the RHEED radar scans depicted in Fig. 1), without regard for the in-plane registry of two materials having quite different lattice constants (this registry can be accommodated by a suitably chosen coincidence lattice, as discussed below).

EBSD is the fastest and most reliable method for definitively determining the crystalline structure and orientation of a single-phase or multiphase crystalline solid.[12,25] In addition, it offers high spatial resolution and thus direct visualization of even nanocrystalline grain/domain structures. Figure 3(a) shows maps of the out-of-plane orientation of the sample grown at 500 °C on GaN(0001), illustrating its pure [101] out-of-plane crystal orientation. Figure 3(c) shows an in-plane orientation map which directly visualizes the Pitsch-Schrader OR for this sample, with three symmetry-equivalent domains rotated by 120° relative to each other.[17,19] Note that the tolerance used to record this micrograph (10°) cannot distinguish between the Pitsch-Schrader and Burgers ORs. We used this high tolerance because of the rather large orientational spread present in each domain, as

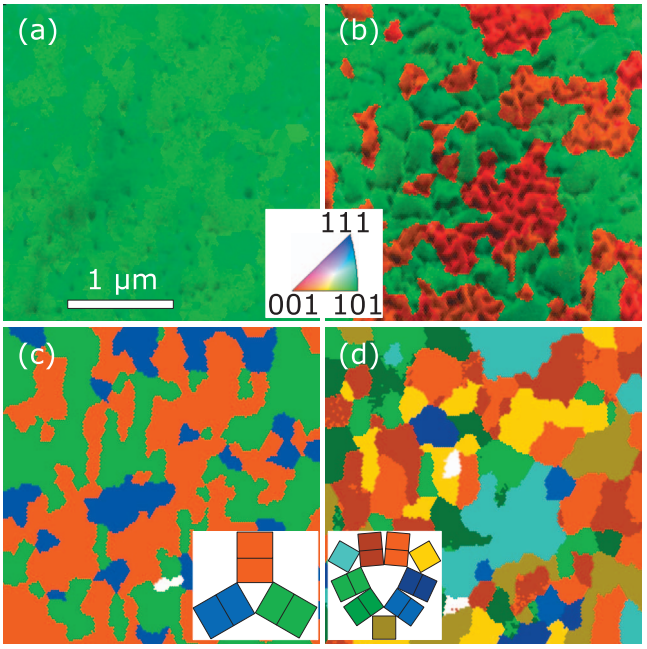

FIG. 3. (Color) Orientation maps as obtained by EBSD. (a) and (b) [(c) and (d)]: out-of-plane [in-plane] orientation maps of the Fe films grown at 500 °C on GaN(0001) and GaN(000$\bar{1}$) substrates, respectively. The inset in (a) and (b) shows an inverse pole figure with the color coding used in the maps. The insets in (c) and (d) schematically depict the orientation of the individual domains with their respective color coding.

seen in Fig. 1(a). Micrographs taken with a smaller tolerance rule out the presence of the Burgers OR.

In comparison, the results for GaN(000$\bar{1}$) shown in Fig. 3(b) clearly exhibit the coexistence of two different out-of-plane orientations, [101] and [001], with roughly the same areal density. The in-plane orientation map in Fig. 3(d) directly reveals domains with the Burgers/Pitsch-Schrader and CoH orientations, respectively. As above, the large tolerance used does not allow us to distinguish between the Pitsch-Schrader and Burgers ORs. Micrographs taken with a smaller tolerance, however, suggest that these two ORs do indeed coexist. To definitively settle this issue HRXRD measurements, to which we now turn, are required.

Figures 4(a) and 4(b) show HRXRD θ-2θ scans containing the major reflections of Fe for the samples on GaN(0001) and GaN(000$\bar{1}$), respectively. Apart from the (0002) [(0006)] reflections of GaN (Al_2O_3), the (101) reflection of α-Fe is present in all scans. In Fig. 4(b), the α-Fe(002) reflection appears in addition, demonstrating the existence of a phase with α-Fe(001)$\|$GaN(0001).

Figures 5(a) and 5(b) compare skew-geometry HRXRD ϕ scans of the GaN$\{10\bar{1}4\}$ and α-Fe$\{211\}$ planes of all samples. For GaN(0001) [Fig. 5(a)], we observe two maxima $\pm 5.3°$ next to each GaN$\{10\bar{1}4\}$ reflection, in perfect agreement with the results obtained by RHEED [cf. Fig. 1(a)]. For the samples grown at 350 and 500 °C on GaN(000$\bar{1}$), we observe two distinct out-of-plane reflections and thus performed in-plane scans with a different inclination angle χ.

For $\chi = 30°$ [the angle between the (101) and (211) planes]

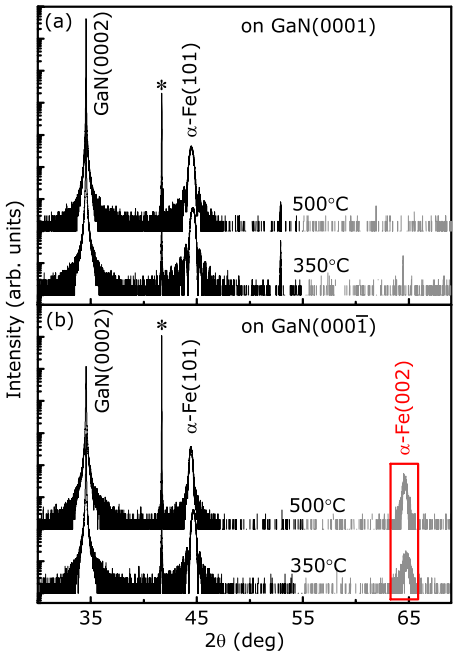

FIG. 4. (Color online) Symmetric HRXRD longitudinal θ-2θ scans of the Fe films grown at 350 and 500 °C on (a) GaN(0001) and (b) GaN(000$\bar{1}$) substrates, respectively. The peak labeled with a star is the Al_2O_3(0006) reflection. The Fe(002) reflection in (b) is outlined.

we find three prominent maxima located at 0 and ±10.5° relative to the GaN{10$\bar{1}$4} reflection, thus reflecting the Burgers OR. However, by fitting Gaussians to these profiles we

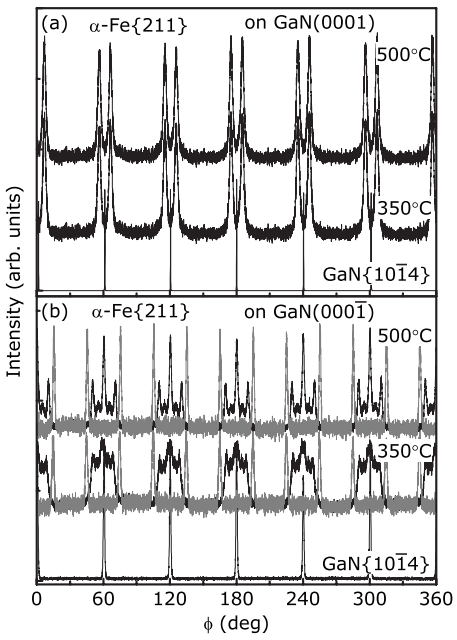

FIG. 5. HRXRD azimuthal ϕ scans of the GaN{10$\bar{1}$4} and α-Fe{211} planes for the structures grown at 350 and 500 °C on (a) GaN(0001) and (b) GaN(000$\bar{1}$) substrates, respectively. The scans were recorded at inclination angles χ of 25.15° (GaN{10$\bar{1}$4}), 30° (black lines), and 35.26° [gray lines in (b)].

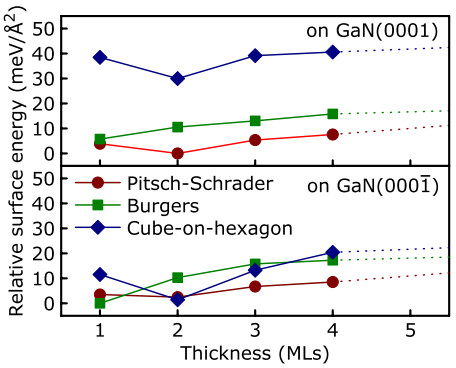

FIG. 6. (Color online) Theoretical surface energies for Fe films of different thickness in MLs grown on Ga- and N-polar surfaces of GaN, in three different orientational relationships. The dotted lines represent linear extrapolations arising from the small residual strain in the bulk (see discussion).

infer also the existence of a small fraction of Pitsch-Schrader domains. The superior angular resolution of HRXRD thus indeed allows us to distinguish between the Pitsch-Schrader and the Burgers OR. For χ=35.26° [the angle between the (001) and (112) planes] two narrow maxima at ±15° relative to the GaN{10$\bar{1}$4} reflection are observed. This result confirms that obtained by RHEED and corresponds to the CoH OR.

We performed a series of DFT calculations to determine the relative stability of the Pitsch-Schrader, Burgers, and cube-on-hexagon ORs for Fe on GaN(0001) and GaN(000$\bar{1}$). In each case, the Fe and GaN in-plane lattice mismatch is so large that simple atomic registry is not physically plausible. Thus, we only assumed registry within a suitable Fe/GaN coincidence lattice,[26] which we construct for each orientation so as to reduce the residual in-plane strain within the Fe film to 3% or less. We show below that these small residual strains do not affect our predictions for the relative stability of the different orientations. The thermodynamic stability of the different ORs rests on the usual criterion of lowest surface energy, here evaluated in the Fe-rich chemical potential condition. Because relative stability may well vary with the thickness of the Fe film, we considered films from 1 to 4 monolayers (MLs) thick. The GaN substrate was represented by a passivated slab of four atomic layers. For GaN(0001) the bulk-terminated surface was used, and for GaN(000$\bar{1}$) Ga-adlayer termination[27] was assumed. Total energies and forces were calculated within the generalized gradient approximation[28] to DFT using projector-augmented-wave potentials.[29,30] All atomic positions were fully relaxed except the final double layer of GaN.

The resulting surface energies, shown in Fig. 6, are consistent with the experimental observations described above. Most importantly, we find that the cube-on-hexagon orientation is energetically competitive on the N-polar surface but is far less likely to occur on the Ga-polar surface. Figure 7 shows the fully relaxed film structure in this new orientation on the N-polar surface.

The DFT results displayed in Fig. 6 for the Ga-polar surface show that the Pitsch-Schrader orientation has the lowest

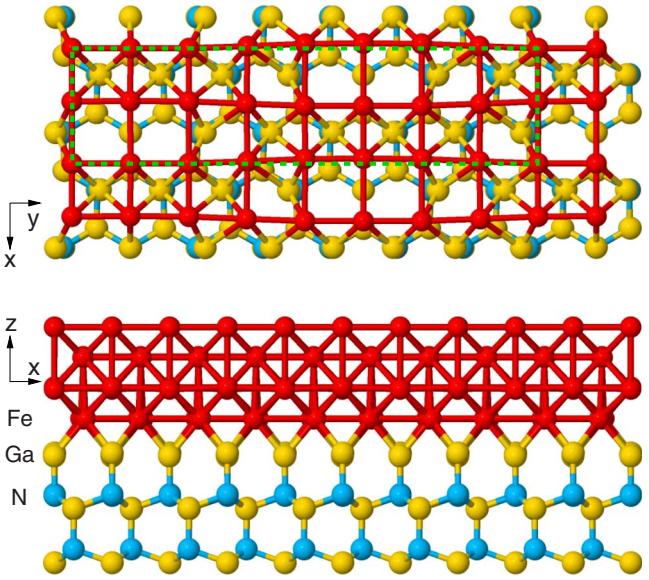

FIG. 7. (Color online) Theoretical equilibrium structure of a four-layer Fe film on the N-polar GaN(000$\bar{1}$) surface in the cube-on-hexagon orientation. The dashed green outline in the top view shows the Fe/GaN coincidence lattice, a $c(2\times7)$ supercell of GaN (at zero strain) and a $c(2\times8)$ supercell of Fe (at residual in-plane strain $\varepsilon_{xx}=-0.018$ and $\varepsilon_{yy}=-0.008$). The upper three Fe layers are omitted in the top view for clarity. The coordinate system is defined as $x\|[11\bar{2}0]$, $y\|[1\bar{1}00]$, and $z\|[0001]$.

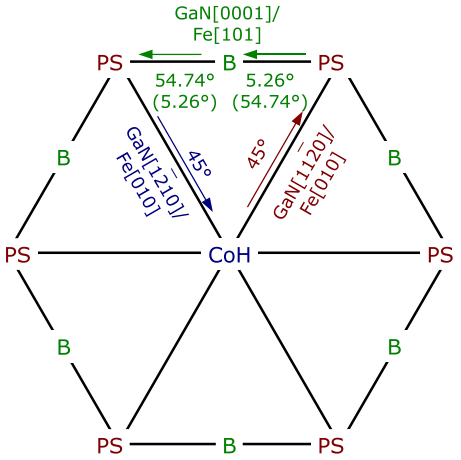

FIG. 8. (Color online) Symmetry diagram showing the relationships between the CoH, PS, and B ORs in bcc/hcp epitaxy. The rotations transforming among the three ORs are indicated.

energy for all Fe film thicknesses, in agreement with its being the only orientation observed on GaN(0001). The behavior on the N-polar surface is more complex, with all three orientations emerging as the most stable at various different film thicknesses. The experimental suppression of the Pitsch-Schrader phase on the N-polar surface suggests that the coexisting Burgers and cube-on-hexagon orientations are locked in by their favorable energetics in the first 1 or 2 MLs, and that with continued growth the Pitsch-Schrader orientation is rendered kinetically inaccessible despite its thermodynamic stability for thicker films. Interestingly, we find that the contribution of the orientation-dependent interface energy to the full surface energy is already converged at 3–4 MLs: beyond this thickness the surface energies are nearly constant (dotted lines), except for the very small residual strain contribution arising from the coincidence lattices. This establishes the important point that any meaningful distinctions among the different orientations must be already established in the first 1–3 MLs, and thus that thicker films need not be studied in order to identify those distinctions.

Finally, Fig. 8 shows a symmetry diagram[20] connecting the CoH, Pitsch-Schrader and Burgers ORs in bcc/hcp systems as observed in our experiments. The Pitsch-Schrader OR can be produced from the CoH OR by a 45° rotation around the Fe[010]/GaN[11$\bar{2}$0] axis to bring Fe(101) in coincidence with GaN(0001). The Burgers OR, in turn, can be produced from the Pitsch-Schrader OR by a 5.26°(54.74°) rotation around the Fe[101]/GaN[0001] axis to bring Fe[1$\bar{1}\bar{1}$]([11$\bar{1}$]) in coincidence with GaN[1$\bar{2}$10]/([11$\bar{2}$0]), and vice versa. The high-symmetry CoH orientation is therefore the central—and heretofore missing—link in the symmetry diagram for bcc/hcp heteroepitaxy.

We thank Jens Herfort and Achim Trampert for critically reading the manuscript. This work was supported in part by the U.S. Office of Naval Research. Computations were performed at the DoD Major Shared Resource Center at AFRL.

*gaocunx@pdi-berlin.de

[1] E. C. Bain, Trans. Am. Inst. Min. Metall. Eng. **70**, 25 (1924).
[2] G. Kurdjumow and G. Sachs, Z. Phys. **64**, 325 (1930).
[3] G. Wassermann, Arch. Eisenhüttenwes. **6**, 347 (1933).
[4] W. G. Burgers, Physica (Amsterdam) **1**, 561 (1934).
[5] Z. Nishiyama, Sci. Rep. Res. Inst. Tohoku Univ. **23**, 637 (1934).
[6] A. B. Greninger and A. R. Troiano, Met. Trans. **185**, 590 (1949).
[7] K. H. Jack, J. Iron Steel Inst., London **169**, 26 (1951).
[8] W. Pitsch and A. Schrader, Arch. Eisenhüttenwes. **29**, 715 (1958).
[9] W. Pitsch, Philos. Mag. **4**, 577 (1959).
[10] D. I. Potter, J. Less-Common Met. **31**, 299 (1973).
[11] T. Furuhara, N. Sugita, and T. Maki, ISIJ Int. **36**, 584 (1996).
[12] Y. L. He, S. Godet, and J. J. Jonas, J. Appl. Crystallogr. **39**, 72 (2006).
[13] D. E. Laughlin and B. Y. Wong, IEEE Trans. Magn. **27**, 4713 (1991).
[14] S. Andrieu, M. Piecuch, and J. Bobo, Phys. Rev. B **46**, 4909 (1992).
[15] O. Hellwig, K. Theis-Bröhl, G. Wilhelmi, A. Stierle, and H. Zabel, Surf. Sci. **398**, 379 (1998).
[16] M. D. Cropper, T. C. Q. Noakes, M. T. Butterfield, and P. Bailey,

Surf. Sci. **594**, 212 (2005).
[17] R. Meijers, R. Calarco, N. Kaluza, H. Hardtdegen, M. Ahe, H. L. Bay, H. Lüth, M. Buchmeier, and D. E. Bürgler, J. Cryst. Growth **283**, 500 (2005).
[18] G. Nowak, A. Remhof, F. Radu, A. Nefedov, H.-W. Becker, and H. Zabel, Phys. Rev. B **75**, 174405 (2007).
[19] C. X. Gao, O. Brandt, H.-P. Schönherr, U. Jahn, J. Herfort, and B. Jenichen, Appl. Phys. Lett. **95**, 111906 (2009).
[20] U. Dahmen, Acta Metall. **30**, 63 (1982).
[21] E. Bauer and J. H. van der Merwe, Phys. Rev. B **33**, 3657 (1986).
[22] A. R. Smith, R. M. Feenstra, D. W. Greve, M. S. Shin, M. Skowronski, J. Neugebauer, and J. E. Northrup, J. Vac. Sci. Technol. B **16**, 2242 (1998).
[23] W. Braun, *Applied RHEED*, Springer Tracts in Modern Physics Vol. 154 (Springer, Berlin, 1999).
[24] C. X. Gao, H.-P. Schönherr, and O. Brandt, Appl. Phys. Lett. **97**, 031906 (2010).
[25] G. Nolze, V. Geist, R. S. Neumann, and M. Buchheim, Cryst. Res. Technol. **40**, 791 (2005).
[26] A. Trampert and K. H. Ploog, Cryst. Res. Technol. **35**, 793 (2000).
[27] D. Segev and C. G. Van de Walle, Surf. Sci. **601**, L15 (2007).
[28] J. P. Perdew, K. Burke, and M. Ernzerhof, Phys. Rev. Lett. **77**, 3865 (1996).
[29] G. Kresse and J. Hafner, Phys. Rev. B **47**, 558 (1993).
[30] G. Kresse and J. Furthmüller, Phys. Rev. B **54**, 11169 (1996).